Design and Control of CRAM: A Highly Articulated Cable-driven Remote Access Manipulator for Confined Space Inspection

Wilhelm Johan Marais[1], **Ali Haydar Göktoğan**[2]
The School of Aerospace, Mechanical and Mechatronic Engineering[1,2]
Australian Centre for Field Robotics[2]
The University of Sydney, Australia
wmar5627@uni.sydney.edu.au[1], a.goktogan@acfr.usyd.edu.au[2]

Abstract

The use of robotics for inspection operations in hazardous environments such as confined spaces has seen significant recent advancement. Removing the need for human entry to such spaces is desirable due to safety and time benefits, with associated cost reduction. Challenges arise when navigating a robotic manipulator in a constrained environment, leading to a need for highly articulated motion and a large number of Degrees of Freedom (DoF). Tendon/cable-driven manipulator systems are used to realise large length-to-diameter ratios by removing the need for lifting the weight of actuators. This paper presents the design of a Cable-driven Remote Access Manipulator (CRAM), which requires only one actuator per DoF and achieves bending angles of $\pm 90°$. CRAM's feeding motion is provided by a linear sliding rail and it has a changeable end effector to be used for a variety of inspection operations. The mechanical design, system architecture and a kinematic control scheme are detailed. A working prototype is presented, with experiments validating the design concept.

1 Introduction

Confined spaces pose unique operational risks for humans during routine inspection operations. Robotic systems are therefore critical to remove the need for human exposure to these dangerous environments. A confined space is defined as one which is geometrically cramped, leading to operational difficulties. The primary example to be considered is the internal wing structure of an aircraft, in which regular inspection is required [Guochen *et al.*, 2014]. Due to the nature of confined spaces and the access difficulties associated with them, slender arm type robots are being used for remote access [Buckingham and Graham, 2010].

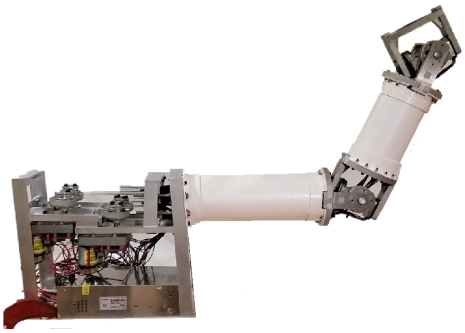

Figure 1: Cable-driven Remote Access Manipulator (CRAM) is a highly articulated robotic, slender manipulator developed to perform maintenance tasks in confined spaces.

These manipulators usually have large length-to-diameter ratios to enable them to access limited workspace areas [Dong *et al.*, 2017; Liu *et al.*, 2016]. Due to the smaller diameter, they have limited space for actuator housing along the arm. Slender arms also generally have a large number of Degrees of Freedoms (DoF) to allow for navigation of complex environments and snake-like motion [Paljug *et al.*, 1995]. Therefore these type of robots are often actuated by cables (also known as tendons), with actuators at the base of the arm. This removes the distributed mass of actuators along the length of the arm, allowing for greater payload capacity and reduced size [S. Hirose, 1991]. Slender arm systems are often mounted on a linear sliding or rotating base, enabling forward translation of the entire manipulator for remote access to confined spaces [Dong *et al.*, 2017]. The use of tendon driven continuum robotic manipulators and pneumatically actuated soft robotics have seen recent development due to the flexibility and compliance safety offered [Zheng Li, 2015]. Continuum robots are classed as hyper-redundant, offering an infinite number of articulation points. This class of robots however lack the rigidity required for long lengths and large payloads relative to discrete structures [G. Robinson, 1999;

Robert J. Webster, 2010].

Rigid articulated systems consist of discrete bending points connected by stiff links. An example of such a tendon driven manipulator is the OC Robotics X125. This system consists of one universal joint (also known as Cardan joint or U-Joint) at each articulation point, offering two coincident DoF. This allows for highly articulated motion, and a high payload capacity [Buckingham and Graham, 2010]. Actuation is achieved through radial arrangement of tendons at each joint. A limitation of this design is the requirement for multiple actuators per DoF and limited bending angle per joint.

Another universal joint mechanism was proposed by [J. Shang and Yang, 2011]. This system has embedded actuators within the arm, with tendons used to transmit power to each joint. This system can achieve large bending angles of $\pm 45°$ per 2-DoF joint. The mass of actuators along the length of the arm limits the payload capacity and number of DoF of the system.

Coupled tendon control [Horigome *et al.*, 2014] allows for only one actuator per DoF. This is achieved by attaching opposing cables for each DoF to the same actuator. This design enable large bending angles and payload capacity. So far, coupled tendon systems have only one DoF per joint, limiting their degree of articulation.

This paper presents a novel new slender manipulator design, a Cable-driven Remote Access Manipulator (CRAM), which realises coupled tendon control with a 2-DoF universal joints, and bending angles of $\pm 90°$. A 4-DoF proof of concept prototype is shown in Figure 1. Section 2 gives an overview of the design of the CRAM system, specifically the base which houses the actuators and electronics, the 2-DoF joint design, and the end effector.

Section 3 details the mechatronic design and signal flow of the system. Section 4 gives a in depth description of the kinematics, particularly the redundant inverse kinematics scheme, and self motion for joint limit avoidance. Section 5 outlines the development of a 4-DoF prototype for validation of the key design concepts, and Section 6 the experimental results for the prototype.

2 Mechanical Design

2.1 System Requirements

The technical requirements for the CRAM system are derived from the primary objective to perform the necessary in-situ inspection operations within an aircraft wing through an access port as depicted in Figure 2. The required manipulator path is shown. To achieve this task the following requirements must be satisfied:

- A minimum arm length of 1000mm to reach the desired inspection areas

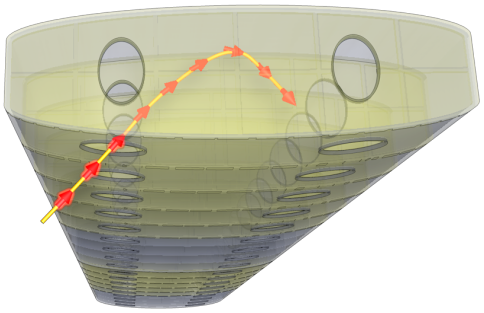

Figure 2: Required path for a proposed manipulator for inspection in a aircraft wing-frame through an access port

- A maximum outer diameter of 150mm to enable access to the given confined space through an access port
- A minimum bending angle per DoF of $\pm 45°$ to allow for the require degree of articulation
- Provision for routing of the wiring of the inspection equipment through centre of the manipulator
- A minimum payload at the tip of 200g to ensure required inspection equipment can be carried
- A minimum of 8-DoF for the required degree of articulation
- The ability to remotely access confined space by means of linear translation along a rail

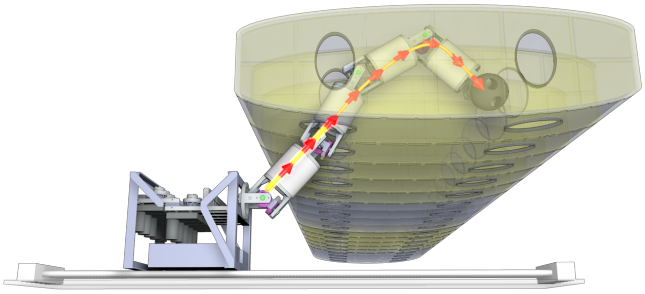

Figure 3: A concept visualisation of the highly articulated CRAM entering into an aircraft wing structure through access ports to perform in-situ inspection

To satisfy these requirements a 12-DoF cable driven system was designed as shown in Figure 3. With actuators placed in the base of the manipulator, this allows for reduced distributed mass along the length of the system and hence a greater length to diameter ratio. The system has a length of 1250mm and a diameter of 115mm, and the base is mounted on a sliding rail.

A universal joint mechanism was used to enable 2-DoF per joint and $\pm 90°$ of motion. CRAM consists of 5

joints providing 10-DoF. An additional 2-DoF are provided by the translating base and a rotating end effector. To minimise the number of actuators to 1 per DoF, a coupled tendon design was implemented using cable pulleys. Bowden tubes are used to decouple each joint such that each joint DoF can be controlled independently by a single motor. This is unlike continuum or comparable universal joint type manipulators which exhibit coupling of DoF to multiple motors. The system is designed for each 2-DoF joint, with corresponding actuators and base mounting, to be modular. This allows for the number of DoF to be changed without changing the design of the system.

2.2 Base Design

The base of the CRAM system is used to house the actuators and the control electronics. High torque servo motors are attached to the base. The motor torque requirement of 30Nm was determined through simulation. CRAM uses ASME-03B servo motors which provide 37Nm and 300° of motion. Only 180° of motion is required at the joint, and hence a mechanical advantage of 1.67 is generated through appropriate pulley sizing. Therefore 61Nm, double the required torque, can be generated at each joint assuming frictionless transmission. In reality, Bowden tube transmissions exhibit high frictional losses and hence high motor torque is required to compensate.

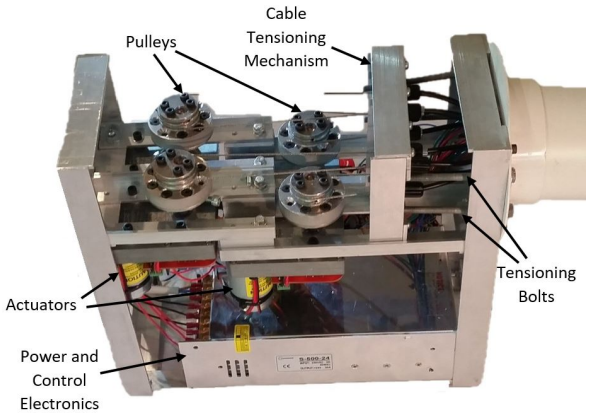

Figure 4: Photo of CRAM base, showing pulleys, actuators and cable tensioning mechanism

A cable tensioning mechanism is used to achieve the desired cable tension for control. Figure 4 shows the cable routing around each motor pulley and the cable tensioning mechanism. The tensioning process involves tightening a set of bolts which pull on the cables.

The base is mounted on a linear rail. A stepper motor drives a rotating ball nut mechanism. Thus all actuators, power and control electronics are housed within the base.

2.3 Joint Design

Several considerations are addressed in the joint design. These include minimising joint backlash, mounting of encoders, and consideration of cable, Bowden tube and inspection equipment routing.

The CRAM joint design is based on a universal joint. Four steel pins are fit into an aluminium octagonal block, forming the central cross. Two identical yoke halves are formed from aluminium sections. The pins connect via flanged bushings to the yoke halves. The use of 2 cable pulleys within the joint allows for large bending angles of each DoF of ±90°. A CAD model of a single 2-DOF joint and a manufactured joint are shown in Figure 5.

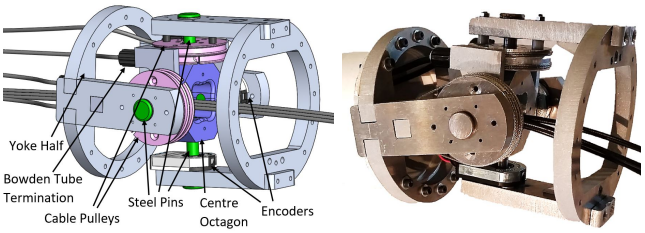

(a) (b)

Figure 5: (a) A CAD model of a 2-DoF CRAM joint, (b) a close up view of the joint

Quadrature encoders are mounted on each joint to account for any uncertainty of rotation angle due to backlash in the cable driven mechanism. These are AMT102 through hole mount components, fixed to the yoke halves. The encoders measure the rotation of the pins relative to the yoke halves. The pins are bolted to the central octagonal block to ensure no relative rotation between the parts for reliable angular readings. High torques are generated by high-torque servo actu-

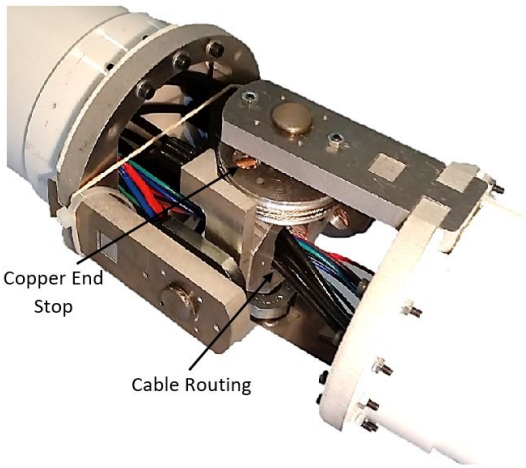

Figure 6: Photo of CRAM joint showing routing Bowden tubes and electrical wires through centre of joint

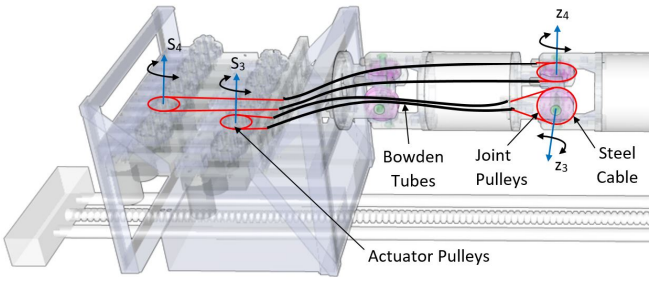

Figure 7: Cable routing of a single 2-DoF joint showing servos S_3 and S_4 which enable rotation about z_3 and z_4 through a coupled tendon mechanism

ators. High tension cables assures that the generated torques are effectively transferred to the joints. This leads to large resultant forces on each of the joint sections. In order to withstand high pulling forces at the joint, all aluminium parts have a minimum thickness of 10mm. Furthermore, joint compliance was reduced by press fitting all parts together. The mass of one joint is 0.83kg. Further refinements can be made to optimise the mass of each joint.

Bowden tube terminations are through standard screw terminals, mounted in line with corresponding cable pulleys. The Bowden tubes used are 4mm diameter. 1.5mm 7×7 wire rope, with a tensile strength of 1.2kN is used for force transmission. The cables are terminated within each pulley using a crimped copper end-stop, providing a holding force of 90% of the wire strength.

Bowden tube, electronics and inspection equipment wiring, are routed through the joint via a hole through the centre of the joint. This minimises the bending of the Bowden tubes, which is necessary for reducing cable friction. A photo of the cable routing can be seen in Figures 6 and 7.

2.4 End Effector

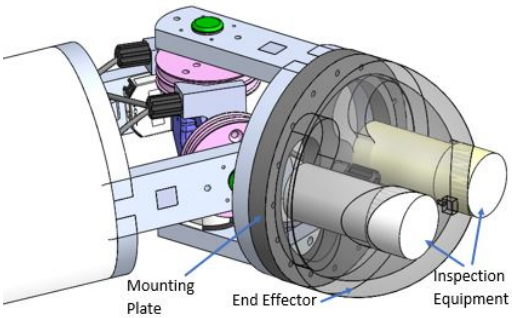

Figure 8: CRAM end effector, enabling a rotate degree of freedom and mounting of inspection equipment

The tip of the CRAM system provides a final DoF, a rotation along the axis of the tip direction. A torque transmission wire, routed through a Bowden cable is used. A plate mounted to the final yoke half by a flanged bushing enables the rotation. The rotating plate allows for mounting of a range of different end effectors. The 3D printed end effector shown in Figure 8 is designed to house an endoscopic camera and a light source.

3 System Architecture

The layout of the system architecture is given in Figure 9. The system is split into two primary sections, the external control sections, and the CRAM system. The primary control loop is run on a Simulink application, with user input from a gamepad. The control scheme is

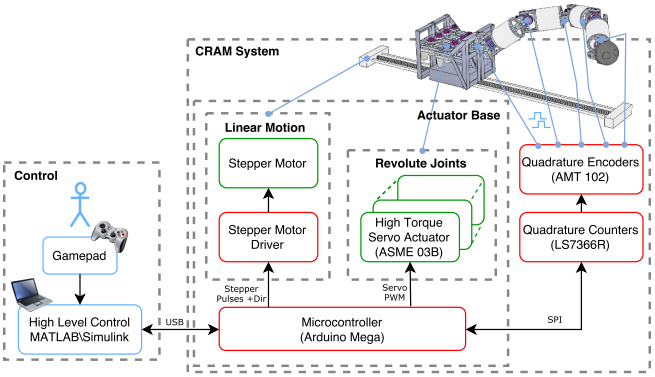

Figure 9: System architecture of the CRAM

run on a laptop for a high iteration frequency of 100Hz for the feedback loop. Serial data is sent from the laptop to a microcontroller which is used to interface with low level hardware. Stepper pulses are sent to a driver and stepper motor for linear motion, and servo pulses are sent to servo motors for joint motion.

Quadrature encoders outputting 2048 pulses per revolution are mounted on each joint. The pulses are read by dedicated 32 bit LS7366R counters, with a Serial Peripheral Interface (SPI) bus connection to the microcontroller. Each servo motor consists of a closed loop controller via a potentiometer mounted on the servo output shaft. The laptop sends desired joint angles of each motor to the microcontroller via serial, and receives encoder angles of each DoF.

4 Kinematics

4.1 Forward Kinematics

Forward kinematics was solved using standard DH parameters. A setup of the coordinate frames is shown in Figures 10 and 11. The DH parameters of CRAM are tabulated in Table 1.

The transformations between frames are given by composed translation and rotation matrices. These matrices

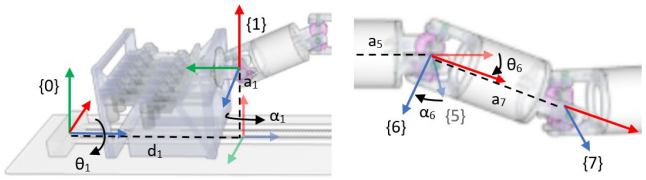

Figure 10: Setup of DH parameters showing transformations between frames with x, y and z axes

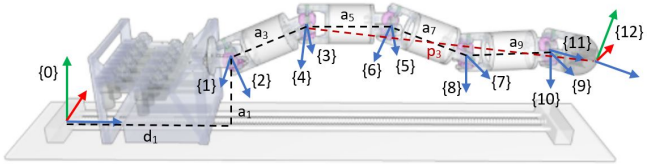

Figure 11: z axes of frames $\{0\}$ to $\{12\}$ showing the axis of translation/rotation for each DoF

are $T_z(d_j)$ a translation along z_{j-1}, $T_{rz}(\theta_j)$ a rotation about z_{j-1}, $T_x(a_j)$ a translation along x_j, and $T_{Rx}(\alpha_j)$ a rotation about x_j.

$$T_z(d_j) = \begin{pmatrix} 1 & 0 & 0 & 0 \\ 0 & 1 & 0 & 0 \\ 0 & 0 & 1 & d_j \\ 0 & 0 & 0 & 1 \end{pmatrix} \tag{1}$$

$$T_{rz}(\theta_j) = \begin{pmatrix} cos(\theta_j) & -sin(\theta_j) & 0 & 0 \\ sin(\theta_j) & cos(\theta_j) & 0 & 0 \\ 0 & 0 & 1 & 0 \\ 0 & 0 & 0 & 1 \end{pmatrix} \tag{2}$$

$$T_x(a_j) = \begin{pmatrix} 1 & 0 & 0 & a_j \\ 0 & 1 & 0 & 0 \\ 0 & 0 & 1 & 0 \\ 0 & 0 & 0 & 1 \end{pmatrix} \tag{3}$$

$$T_{Rx}(\alpha_j) = \begin{pmatrix} 1 & 0 & 0 & 0 \\ 0 & cos(\alpha_j) & -sin(\alpha_j) & 0 \\ 0 & sin(\alpha_j) & cos(\alpha_j) & 0 \\ 0 & 0 & 0 & 1 \end{pmatrix} \tag{4}$$

These can be composed into a pose transformation matrix from frame $\{j-1\}$ to $\{j\}$:

$$^{j-1}A_j(\theta_j, d_j, a_j, \alpha_j) = T_z(d_j)T_{Rz}(\theta_j)T_x(a_j)T_{Rx}(\alpha_j) \tag{5}$$

The transformation between the frame of the base $\{0\}$ and any frame $\{i\}$ along the arm is therefore given by the transformations between each frame along the length of the arm.

$$^0A_i = ^0A_1(\theta_1, d_1, a_1, \alpha_1)...^{i-1}A_i(\theta_i, d_i, a_i, \alpha_i) \tag{6}$$

Table 1: Standard DH Parameters for CRAM

Link	$\mathbf{d_j}$ (mm)	$\boldsymbol{\theta_j}$ (rads)	$\mathbf{a_j}$ (mm)	$\boldsymbol{\alpha_j}$ (rads)	Joint Limit (mm) or (rads)
1	d_1 + 500	$\pi/2$	105	$-\pi/2$	0-1300
2	0	$-\pi/2 + \theta_2$	0	$\pi/2$	$-\pi/2$ - $\pi/2$
3	0	θ_3	250	$-\pi/2$	$-\pi/2$ - $\pi/2$
4	0	θ_4	0	$\pi/2$	$-\pi/2$ - $\pi/2$
5	0	θ_5	250	$-\pi/2$	$-\pi/2$ - $\pi/2$
6	0	θ_6	0	$\pi/2$	$-\pi/2$ - $\pi/2$
7	0	θ_7	250	$-\pi/2$	$-\pi/2$ - $\pi/2$
8	0	θ_8	0	$\pi/2$	$-\pi/2$ - $\pi/2$
9	0	θ_9	250	$-\pi/2$	$-\pi/2$ - $\pi/2$
10	0	θ_{10}	0	$\pi/2$	$-\pi/2$ - $\pi/2$
11	0	$\pi/2 + \theta_{11}$	0	$\pi/2$	$-\pi/2$ - $\pi/2$
12	69	$\pi + \theta_{12}$	0	0	$-\pi/2$ - $\pi/2$

4.2 Inverse Kinematics

The inverse kinematics was solved in a Matlab/Simulink model. The model is shown in Figure 12. The primary outer feedback loop generates the require joint state vector $\mathbf{q}$, for a given desired pose $\mathbf{x}$.

$$\mathbf{q} = \begin{pmatrix} q_1 \\ \vdots \\ q_{12} \end{pmatrix} = \begin{pmatrix} d_1 \\ \theta_2 \\ \vdots \\ \theta_{12} \end{pmatrix} \tag{7}$$

$$\mathbf{x} = \begin{pmatrix} x \\ y \\ z \\ R_x \\ R_y \\ R_z \end{pmatrix} \tag{8}$$

where x, y, z is the spatial position in mm and R_x, R_y, R_z are the roll, pitch and yaw rotations in radians of the end effector frame $\{12\}$ in the base frame $\{0\}$.

Since CRAM has 12-DoF, it is classed as a kinematically redundant manipulator. This class of robots generally have an infinite number of inverse kinematics solutions $\mathbf{q}$ for a given end effector pose $\mathbf{x}$. Therefore explicit

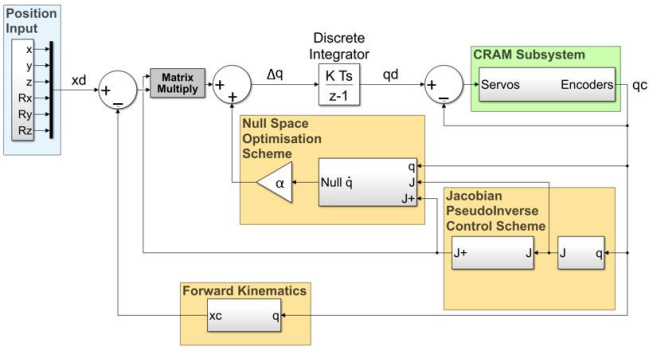

Figure 12: Inverse kinematic control scheme running on a Simulink application

analytic solutions generally do not exist, and iterative numerical techniques are used. The inverse kinematics for the CRAM system was solved using the manipulator Jacobian pseudoinverse [Charles A. Klein, 1983].

This is done by iteratively solving the Jacobian pseudoinverse equation given by

$$\dot{\mathbf{q}} = J^{+}\dot{\mathbf{x}} \tag{9}$$

where J is the Jacobian, J^{+} is the Jacobian pseudoinverse, $\dot{\mathbf{q}}$ is the joint velocity, and $\dot{\mathbf{x}}$ is the velocity of the end effector. This equation can be discretised to give

$$\Delta\mathbf{q} = J^{+}\Delta\mathbf{x} \tag{10}$$

where $\Delta\mathbf{x}$ is the pose error, and $\Delta\mathbf{q}$ is the joint error. This equation is valid given small iteration time-steps. The pose error is given by

$$\Delta\mathbf{x} = \mathbf{x}_d - \mathbf{x}_c \tag{11}$$

where $\mathbf{x}_d$ is the desired pose and $\mathbf{x}_c$ is the current pose. The joint errors $\Delta\mathbf{q}$ can be summed at each time-step s to give

$$\mathbf{q}_d(t) = \sum_{s=0}^{t} \Delta\mathbf{q}(s)\Delta t \tag{12}$$

where Δt is the time-step duration and $\mathbf{q}_d$ is the vector of desired joint angles. This is implemented as a discrete integral in Figure 12. Encoder readings at each joint allow for closed loop control of each servo angle to ensure the current joint angles $\mathbf{q}_c$ match $\mathbf{q}_d$.

The desired pose $\mathbf{x}_d$ is input by the user in real-time through a gamepad. The current pose $\mathbf{x}_c$ of the end effector is found by the matrix ${}^{0}A_{12}$ in (6).

$$\begin{pmatrix} x_c \\ y_c \\ z_c \\ 1 \end{pmatrix} = \begin{pmatrix} x_{12} \\ y_{12} \\ z_{12} \\ 1 \end{pmatrix} = ({}^{0}A_{12}) \begin{pmatrix} 0 \\ 0 \\ 0 \\ 1 \end{pmatrix} \tag{13}$$

To find the roll, pitch and yaw angles,

$$\begin{aligned} R_x &= atan2(\frac{-A_{2,3}}{A_{3,3}}) \\ R_y &= atan2\Big(\frac{A_{1,3}}{cos(R_x)A_{3,3} - sin(R_x)A_{2,3}}\Big) \\ R_z &= atan2(\frac{-A_{1,2}}{A_{1,1}}) \end{aligned} \tag{14}$$

where $A_{i,j}$ referes to matrix element i, j of ${}^{0}A_{12}$.

Calculation of the Jacobian for CRAM is computed at each time-step according to joint angles given by encoder readings.

The Jacobian for CRAM takes the form

$$\begin{aligned} J &= \begin{pmatrix} \partial x_0/\partial q_0 & \cdots & \partial x_0/\partial q_{11} \\ \vdots & \ddots & \vdots \\ \partial x_5/\partial q_1 & \cdots & \partial x_5/\partial q_{11} \end{pmatrix} \\ &= \begin{pmatrix} z_0 & z_1 \times p_1 & \cdots & z_{11} \times p_{11} \\ 0 & z_1 & \cdots & z_{11} \end{pmatrix} \end{aligned} \tag{15}$$

where $z_0, \cdots, z_{11}$ are the joint axes for frames $\{0 \cdots 11\}$ with respect to frame $\{0\}$, and $p_0, \cdots, p_{11}$ are the vectors from frames $\{0 \cdots 11\}$ to the end effector frame $\{12\}$ with respect to frame $\{0\}$. The vectors vector $z_0, \cdots, z_{11}$ and p_3 are shown in Figure 11.

Each value of z and p can be found using the forward kinematics and DH parameters for any configuration.

$$\begin{pmatrix} z_i \\ 1 \end{pmatrix} = ({}^{0}A_i) \begin{pmatrix} 0 \\ 0 \\ 1 \\ 0 \end{pmatrix} \tag{16}$$

$$p_i = \begin{pmatrix} x_{12} \\ y_{12} \\ z_{12} \\ 1 \end{pmatrix} - ({}^{0}A_i) \begin{pmatrix} 0 \\ 0 \\ 0 \\ 1 \end{pmatrix} \tag{17}$$

The calculation of z and p at every time-step according to the angles as determined by the joint encoders ensures a fast convergence time for the inverse kinematics scheme.

4.3 Null Space Joint Optimisation

Since the Jacobian is a 6×12 matrix, it maps from a 12-dimensional joint space $\mathbf{q}$ to a 6-dimensional task space $\mathbf{x}$. Thus a basis of dimension 6 gets mapped to $\mathbf{x}$ and another basis of dimension 6, the null space, gets mapped to $\mathbf{0}$. Any joint movements which exist purely in the null space produce no end effector motion [Charles A. Klein, 1983].

The null space vectors can be extracted from a given desired $n \times 1$ joint velocity vector $H(\mathbf{q}, t)$. This is given by

$$(I_n - J^{+}J)H(\mathbf{q}, t) \tag{18}$$

where I_n is the $n \times n$ identity matrix, where n is the number of DoF. Therefore the new control scheme can be written as

$$\Delta\mathbf{q} = J^{+}\Delta\mathbf{x} + \alpha((J^{+}J - I_n)H(\mathbf{q}, t) \tag{19}$$

where α is a positive gain constant which is tuned empirically. $H(\mathbf{q}, t)$ can be chosen to optimise a joint configuration based on some criteria. For the CRAM system $H(\mathbf{q}, t)$ is used to minimise joint angles and keep them

within mechanical limits. This is achieved by extracting the vector which will reduce the maximum joint angle.

$$H(\mathbf{q},t) = \begin{cases} sgn(\mathbf{q})\ max|\mathbf{q}|, & max|\mathbf{q}| > \frac{\pi}{4} \\ 0 & max|\mathbf{q}| \leq \frac{\pi}{4} \end{cases} \quad (20)$$

where the centre of motion for each joint is 0. Here the function max returns a velocity vector containing only the maximum joint angle, and sgn preserves the required direction of motion for angle minimisation. For prismatic joint q_0 responsible for base translation, the measure was scaled as

$$q_0 \rightarrow \left(\frac{q_0}{q_a} - 1\right)\frac{\pi}{2} \quad (21)$$

where q_a is the centre of q_0, to create consistent joint scaling. A dead zone of $\pm\pi/4$ is implemented to prevent total straightening of joint. This is implemented to limit the occurrence of kinematic singularities.

5 Prototype Development

5.1 Design of Prototype

A 2 joint, 4-DoF prototype was developed as a proof of design concept. The primary concepts to be verified were

- Controllability of a cable driven system, specifically induced oscillations
- Cable friction, tension, and tensile stength
- The ability of the arm to lift its own weight
- Wire routing for a 2 DoF universal joint mechanism
- Wire routing through a universal joint for successive joints

The system was constructed of water-jet cut and drilled aluminium sections, and steel pins. The parts were press fit and bolted together to reduce joint compliance. The diameter of the prototype is 115mm with a length of 800mm. Rigid PVC parts were used for connecting successive joints together. The servo motors were powered by a high power 24V power supply. The prototype is shown in Figure 1.

5.2 Control of Prototype

The inverse kinematics control scheme was run on a Matlab/Simulink application, as shown in Figure 12. Only the position elements of the end effector pose were considered

$$\mathbf{x} = \begin{pmatrix} x \\ y \\ z \end{pmatrix} \quad (22)$$

Encoder feedback at each joint is used for matching joint angles $\mathbf{q}_c$ to desired joint angles $\mathbf{q}_d$. This is the inner feedback loop in Figure 12, with a P-I controller. The true current joint angles are also used for calculation of the pose error and Jacobian. Thus a cascaded control loop is formed which ensures any backlash within the cable driven mechanism is accounted for.

6 Experimental Results

6.1 Positioning Accuracy

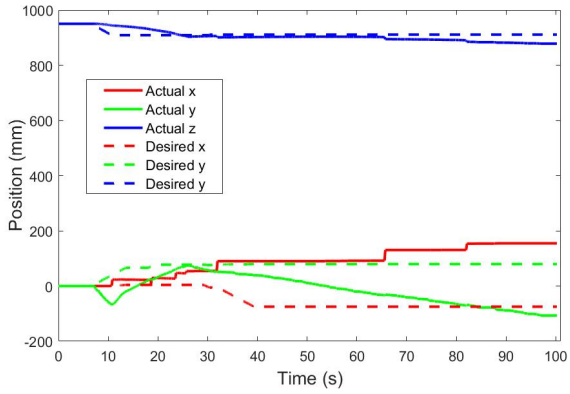

(a) Actual pose and desired pose

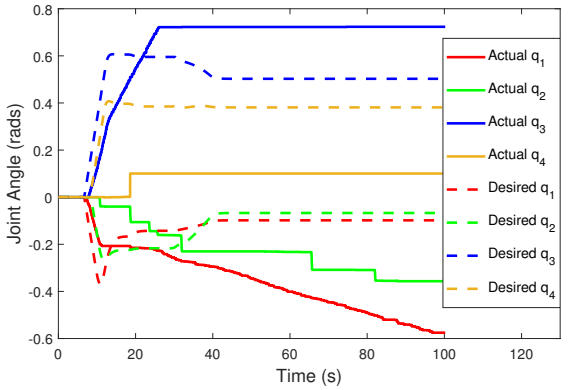

(b) Actual joint angles and desired joint angles

Figure 13: Operation of the 4-DoF prototype with no encoder feedback

The positioning accuracy of the 4-DoF prototype was determined to verify the cable driven concept. Graphs of the actual pose and desired pose, as well as the actual joint angles and desired joint angles are shown for two cases. The first case shown in Figures 13a and 13b is the system performance without encoder feedback. The graphs show the divergence of the actual and desired pose over time, as well as the actual and desired joint angles. This is due to the backlash which is present in the cable mechanism. This motivates the need for encoder mounting on each joint to allow for closed loop control.

The second case shown in Figures 14a and 14b is the system performance with encoder feedback. Figure 14a

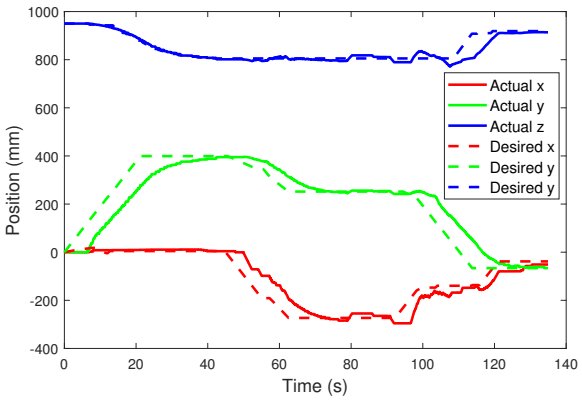

(a) Actual pose and desired pose

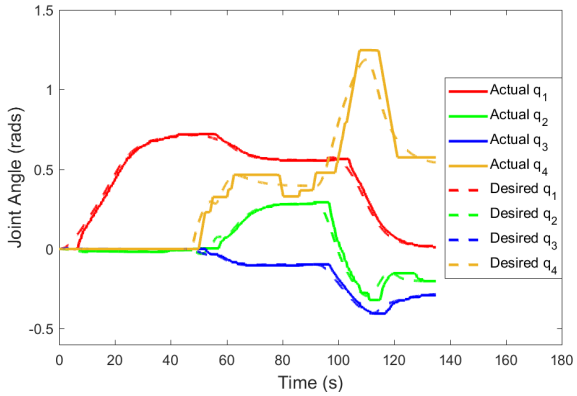

(b) Actual joint angles and desired joint angles

Figure 14: Operation of the 4-DoF prototype with encoder feedback

shows the convergence to the desired pose and the effectiveness of both the inverse kinematics control scheme and the cable-driven joints. Figure 14b shows the improved matching of joint angles to desired joint angles. High tension in the cable mechanism, reduces oscillations within the system.

The CRAM prototype is shown during operation in Figure 15. The routing of electrical wires and Bowden tubes through the centre of each joint is shown to be viable even for large bending angles.

6.2 Loading Conditions

Experiments were done on the loading conditions of the CRAM system. The aim was to determine the feasibility of adding additional joints. The mass of additional joints amounts to 2.5kg. A 5kg mass was attached to the end of the fully stretched arm. This created a large amount of additional loading on the first joint, confirming that the system can support the distributed weight of additional joints. Figures 16a and 16b show the pose and desired pose of the prototype with an additional 5kg

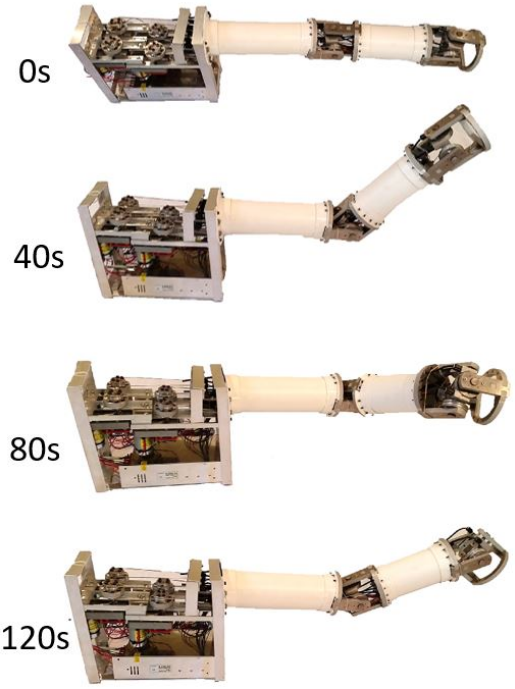

Figure 15: CRAM Prototype during operation

load attached to the end. There is a noticeable effect on the pose convergence time with the additional mass, yet the effect is not significant enough to effect performance.

7 Conclusion

The CRAM system has been designed to perform inspection in confined spaces. The specific scenario from which the system requirements are derived is for inspection within an aircraft wing structure. To achieve this CRAM has 12-DoF and a large length to diameter ratio. This requires the use of a cable driven mechanism to remove the mass of actuators within the arm. The kinematically redundant system is controlled by means of the Jacobian pseudoinverse, with self motion computed for joint limit avoidance.

A 4-DoF prototype has been developed to test several of the key design concepts. The experimental results demonstrate the validity of the mechanical design, and well as the inverse kinematics scheme. The importance of having quadrature encoders mounted directly on each joint is also shown. This accounts for backlash which is present in the cable-driving mechanism. The loading conditions of the prototype were also tested. This confirms the ability of the system to have additional joints mounted.

Future work aims to implement additional joints and linear sliding motion. The conduction of in-situ trails provides further opportunities to develop control methods in unstructured environments.

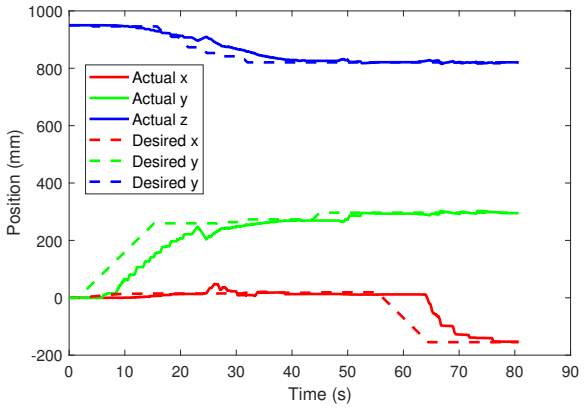

(a) Actual pose and desired pose

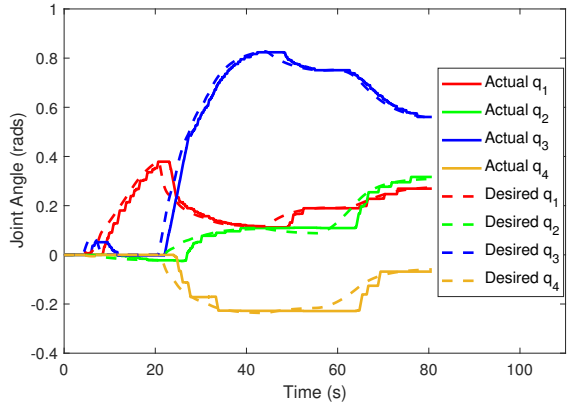

(b) Actual joint angles and desired joint angles

Figure 16: Operation of the 4-DoF prototype with an additional 5kg load

References

[Buckingham and Graham, 2010] R. O. Buckingham and A. C. Graham. Dexterous manipulators for nuclear inspection and maintenance - Case study. In *2010 1st International Conference on Applied Robotics for the Power Industry*, pages 1–6, Oct 2010.

[Charles A. Klein, 1983] Ching-Hsiang Huang Charles A. Klein. Review of pseudoinverse control for use with kinematically redundant manipulators. In *IEEE Transaction on Systems, Man, and Cybernetics*, pages 245 – 250, March 1983.

[Dong *et al.*, 2017] X. Dong, D. Axinte, D. Palmer, S. Cobos, M. Raffles, A. Rabani, and J. Kell. Development of a slender continuum robotic system for on-wing inspection/repair of gas turbine engines. *Robotics and Computer-Integrated Manufacturing*, 44(Supplement C):218 – 229, 2017.

[G. Robinson, 1999] J.B.C. Davies G. Robinson. Continuum robots - a state of the art. In *1999 IEEE International Conference on Robotics and Automation (ICRA)*, pages 62–66, May 1999.

[Guochen *et al.*, 2014] Niu Guochen, Wang Li, Gao Qingji, and Hu Dandan. Path-tracking algorithm for aircraft fuel tank inspection robots. *International Journal of Advanced Robotic Systems*, 11(5):82, 2014.

[Horigome *et al.*, 2014] A. Horigome, H. Yamada, G. Endo, S. Sen, S. Hirose, and E. F. Fukushima. Development of a coupled tendon-driven 3D multi-joint manipulator. In *2014 IEEE International Conference on Robotics and Automation (ICRA)*, pages 5915–5920, May 2014.

[J. Shang and Yang, 2011] C. Payne J. Clark M.H. Sodergren A. Darzi J. Shang, D.P. Noonan and G.-Z. Yang. An articulated universal joint based flexible access robot for minimally invasive surgery. In *2011 IEEE International Conference on Robotics and Automation (ICRA)*, pages 1147–1152, May 2011.

[Liu *et al.*, 2016] Shuntao Liu, Zhixiong Yang, Zhijun Zhu, Liangliang Han, Xiangyang Zhu, and Kai Xu. Development of a dexterous continuum manipulator for exploration and inspection in confined spaces. *The Industrial Robot*, 43(3):284–295, 2016.

[Paljug *et al.*, 1995] E. Paljug, T. Ohm, and S. Hayati. The JPL serpentine robot: a 12-DOF system for inspection. In *Proceedings of 1995 IEEE International Conference on Robotics and Automation*, volume 3, pages 3143–3148 vol.3, May 1995.

[Robert J. Webster, 2010] Bryan A. Jones Robert J. Webster. Design and kinematic modelling of constant curvature continuum robots: A review. *The International Journal of Robotics Research*, 29:16611683, June 2010.

[S. Hirose, 1991] S. Ma S. Hirose. Coupled tendon-driven multijoint manipulator. In *Proceedings of 1991 IEEE International Conference on Robotics and Automation*, volume 2, pages 1268 – 1275, April 1991.

[Zheng Li, 2015] Hongliang Ren Philip W.Y.Chiu Ruxu Du Zheng Li, Haoyong Yu. A novel constrained tendon-driven serpentine manipulator. In *2015 IEEE/RSJ International Conference on Intelligent Robots and Systems (IROS)*, pages 62–66, Sept 2015.